Title
Effect of overturning circulation on long equatorial waves: a low frequency cutoff

Journal
Journal of the Atmospheric Sciences, 75(5)

ISSN
0022-4928

Authors
Back, Amanda
Biello, Joseph A

Publication Date
2018-05-01

DOI
10.1175/jas-d-17-0173.1

Peer reviewed

Effect of Overturning Circulation on Long Equatorial Waves: A Low-Frequency Cutoff

AMANDA BACK[a] AND JOSEPH A. BIELLO

Department of Mathematics, University of California, Davis, Davis, California

(Manuscript received 7 June 2017, in final form 18 February 2018)

ABSTRACT

Zonally long tropical waves in the presence of a large-scale meridional and vertical overturning circulation are studied in an idealized model based on the intraseasonal multiscale moist dynamics (IMMD) theory. The model consists of a system of shallow-water equations describing barotropic and first baroclinic vertical modes coupled to one another by the zonally symmetric, time-independent background circulation. To isolate the effects of the meridional circulation alone, an idealized background flow is chosen to mimic the meridional and vertical components of the flow of the Hadley cell; the background flow meridionally converges and rises at the equator. The resulting linear eigenvalue problem is a generalization of the long-wave-scaled version of Matsuno's equatorial wave problem with the addition of meridional and vertical advection. The results demonstrate that the meridional circulation couples equatorially trapped baroclinic Rossby waves to planetary, barotropic free Rossby waves. The meridional circulation also causes the Kelvin wave to develop an equatorially trapped barotropic component, imparting a westward-tilted vertical structure to the wave. The total energy of the linear system is positive definite, so all waves are shown to be neutrally stable. A critical layer exists at latitudes where the meridional background flow vanishes, resulting in a minimum frequency cutoff for physically feasible waves. Therefore, linear Matsuno waves with periods longer than the vertical transport time of the meridional circulation do not exist in the equatorial waveguide. This implies a low-frequency cutoff for long equatorial waves.

1. Introduction

While interactions between atmospheric waves and purely zonal background flows have been the focus of extensive research dating back to Charney (1947), the same cannot be said of the dynamics of waves in the presence of purely meridional background flow. Zonal winds are widely understood to be sources of shear instability, both barotropic and baroclinic, and the stability theory of rotating flows in the presence of zonal shear is far too extensive to summarize.

The main theoretical framework of tropical tropospheric dynamics is Matsuno's theory of neutrally stable waves (Matsuno 1966), which arise as perturbations of a wind-free tropical atmosphere. Tropical dynamics tend to support waves, in contrast to the geostrophically balanced, transport-dominated dynamics of the middle latitudes. Since climatological mean zonal winds tend to occur poleward of the tropics in the upper-tropospheric subtropical jet or the weaker lower-troposphere trade winds, and since the meridional gradient of planetary potential vorticity at the equator is stabilizing against shear instability, shear instability due to zonal winds is a less common mechanism in the tropics. Nonetheless, ageostrophic instabilities (Sakai 1989) have been shown to excite both equatorial Rossby waves and the equatorial Kelvin wave if the vertical and meridional shear is strong enough. These instabilities tend to affect smaller length scale waves (e.g., Kelvin–Helmholtz instabilities tend to occur at the highest resolved zonal wavenumbers) or synoptic zonal length scale waves (e.g., in baroclinic instabilities of the subtropical jet). For typical climatological winds in the subtropics, the most relevant effect of zonal wind shear is the coupling of equatorial and midlatitude Rossby waves either through linear instability (Xie and Wang 1996) or through resonant coupling (Wang and Xie 1996; Majda and Biello 2003; Biello and Majda 2004).

However, the deep tropics is the location of the ITCZ, which is the most meridionally concentrated rising air within the troposphere, and the mean zonal winds tend

[a] Current affiliation: Global Systems Division, NOAA/ESRL, Boulder, Colorado.

Corresponding author: Joseph A. Biello, biello@math.ucdavis.edu

DOI: 10.1175/JAS-D-17-0173.1

to be much weaker there than poleward of the ITCZ. This is why, in the Wheeler–Kiladis diagram (Takayabu 1994; Wheeler and Kiladis 1999), the observed wave spectrum can be plotted superimposed with the theoretical Matsuno dispersion relation to show that linear waves in the absence of climatological zonal wind shear account for much of the spectral power in the observations.

This suggests that in the tropical band, the strong meridional circulation could potentially have a greater effect than the comparatively weaker zonal winds. The observed climatological background invites the following question: given the quiescent background (Matsuno 1966) and the zonal wind shear background (Xie and Wang 1996; Wang and Xie 1996), both having been well studied, what is the effect of the meridional convergence and rising air on the classical Matsuno waves?

Matsuno's theory is generally appropriate for tropical waves since the mean zonal flow nearly vanishes in the deep tropics and, as was already mentioned above, observational studies (Takayabu 1994; Wheeler and Kiladis 1999) use Matsuno's theoretical dispersion relation to sort and classify the observed wave spectrum. While observed dispersion relations do match the theoretical framework over a broad range of zonal wavenumbers and time scales, there is significant discrepancy at the longest time scales and largest zonal scales. Examples of this discrepancy include the Madden–Julian oscillation (MJO) (Zhang 2005), the lack of Kelvin waves at the longest scales, and the sparseness in signal associated with zonally long Rossby waves (Kiladis et al. 2011). In the following, we will show that it is precisely on the longest zonal tropical waves that the meridional convergence in the climatology has its greatest effect.

Biello and Majda (2010) developed the intraseasonal multiscale moist dynamics (IMMD) theory in order to understand which scales in the tropics are affected by background shear and which scales are affected by upscale fluxes of momentum, temperature, and moisture from the synoptic scales. It is a generalization of Majda and Klein's intraseasonal planetary equatorial synoptic-scale dynamics (IPESD) framework (Majda and Klein 2003), which was used in Biello and Majda (2004) to study the effects of upscale transport of temperature and momentum from synoptic to planetary scales as a model of the MJO. Beyond its applicability to the MJO, IMMD is a long-time-scale theory of tropical circulation that uses multiple scale asymptotics to extend the linear theory of Matsuno (1966) to intraseasonal time scales and includes the effects of zonal and meridional climatological winds arising from the Hadley circulation.

On the zonally long scales, the equatorial waveguide creates waves that are meridionally confined. The planetary-scale waves in the IMMD theory are described by the long-wave-scaled equatorial primitive equations in the presence of advection by a background, incompressible flow with components in all three dimensions (zonal, meridional, and vertical):

$$U\frac{\partial}{\partial x}+V\frac{\partial}{\partial y}+W\frac{\partial}{\partial z}, \quad \text{where} \quad \frac{\partial U}{\partial x}+\frac{\partial V}{\partial y}+\frac{\partial W}{\partial z}=0. \tag{1}$$

In any long-wave theory, the meridional coordinate is measured in units of the equatorial deformation scale of 1500 km, reflecting the confinement of the equatorial waveguide. The vertical coordinate is measured in units of 5 km, reflecting the fact that the troposphere is approximately $5\pi \approx 16$ km high in the tropics (the factor of π arises from projecting on vertical baroclinic modes). Since we wish to describe zonally long waves, the zonal coordinate is measured in units of 10 times the deformation scale, 15 000 km. This ratio is determined by the observed ratio of the strength of diabatic heating resolved on the planetary scale compared to that resolved on the synoptic scales. The details of this scaling and the multiscale theories that result can be found in Biello and Majda (2010).

One of the most important results of the IMMD asymptotic theory, and a result that many researchers have not yet appreciated, is that the anisotropic scaling described in the previous paragraph also creates an anisotropic scaling of the three components of the velocity field. Therefore advection by a $50\,\mathrm{m\,s^{-1}}$ zonal wind, a $5\,\mathrm{m\,s^{-1}}$ meridional wind, and a $1.6\,\mathrm{cm\,s^{-1}}$ vertical uplift each correspond to a similar-sized term in the linear theory of equatorial waves. This is a consequence of the fact that the time scales of the parcel trajectories that these different components of advection describe are all the same,

$$\frac{50\,\mathrm{m\,s^{-1}}}{15\,000\,\mathrm{km}}\sim\frac{5\,\mathrm{m\,s^{-1}}}{1500\,\mathrm{km}}\sim\frac{1.6\,\mathrm{cm\,s^{-1}}}{5\,\mathrm{km}}\sim(3.6\,\mathrm{days})^{-1}, \tag{2}$$

which they must be in order for each to have the potential to participate equally in the incompressibility constraint [Eq. (1)]. Put more succinctly, a parcel of fluid in such a three-dimensional flow would traverse one-third of the vertical extent of the troposphere, 1500 km in the meridional direction and 15 000 km in the zonal direction, all in the same time. In this paper, we restrict our attention to a zonally symmetric meridional circulation that would create zonally symmetric subtropical jets and trade winds. Therefore, the zonal derivative of the zonal wind is zero in all the cases we consider, meaning that the background circulation is incompressible in the meridional–vertical plane.

In Earth's troposphere, the meridional transport of angular momentum by the Hadley cell generates a sizable zonal wind manifested in the subtropical jets and

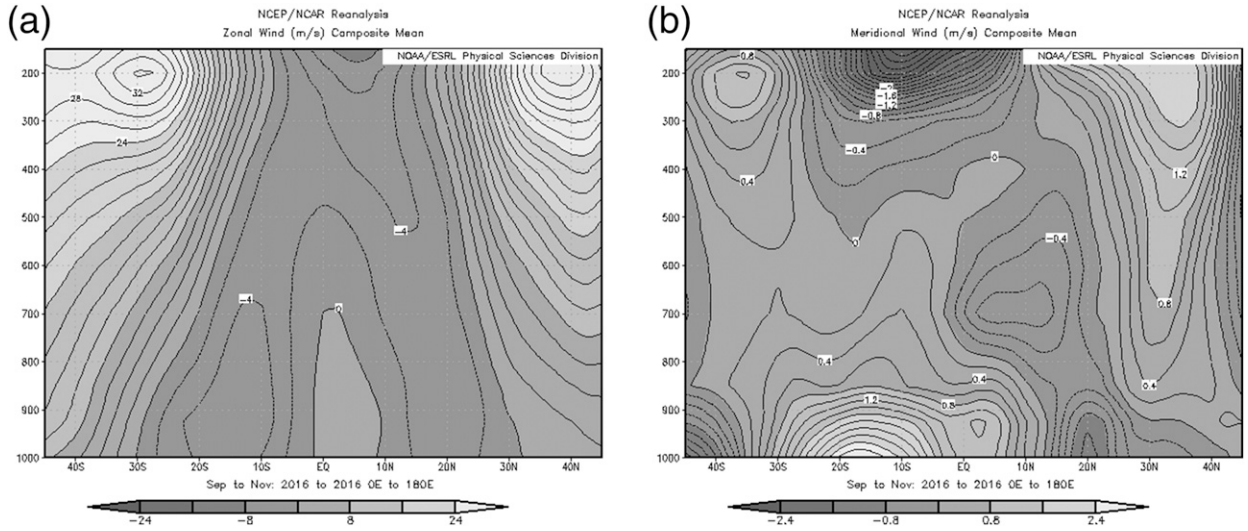

FIG. 1. NCEP reanalysis of averaged (a) zonal and (b) meridional winds plotted from 45°S to 45°N, throughout the depth of the troposphere, from 1000 to 150 hPa (Kalnay 1996). The average is taken over the autumnal equinox months of September, October, and November 2016 and over the Eastern Hemisphere (0°–180°E). Images are provided by the NOAA/ESRL Physical Sciences Division, Boulder, Colorado (http://www.esrl.noaa.gov/psd/). In the long-wave scaling, 3 m s^{-1} meridional flow has the same effect on the linear theory as 30 m s^{-1} zonal flow. It also is clear that the strongest meridional flow is closer to the equator than the strongest zonal flow, and thereby should have an important effect on long equatorial waves.

lower-troposphere trade winds. The specific structure of the subtropical jets and trade winds depends on the form of the angular momentum dissipation through baroclinic instability (Schneider 2006). Observations show (see Fig. 1) that, averaged over intraseasonal time scales and planetary length scales, the subtropical zonal jets attain speeds of 30 m s^{-1} whereas the maximum meridional velocities range from 2.5 m s^{-1} near the bottom to 3.5 m s^{-1} near the top of the troposphere. That these magnitudes are consistent with the relative magnitudes of the long-wave scaling is no coincidence since the tropics do have the necessary separation of magnitudes of diabatic heating that justifies this ratio. What is clear from Fig. 1 is that the strongest meridional velocities occur within 1500 km of the equator. On the other hand, comparable zonal velocities are only attained in the upper troposphere (300 hPa) at distances of about 3000 km from the equator.

The equatorial Kelvin and the first baroclinic equatorial Rossby waves are both generated and trapped within one equatorial deformation radius (1500 km) of the equator. Much research (e.g., Wang and Xie 1996; Biello and Majda 2004) has focused on the effect of zonal winds (both vertical and meridional shear) on equatorially trapped waves. Zonal wind imparts instability to the equatorial Rossby waves and provides a source of coupling to midlatitude Rossby waves. However, equatorial Kelvin waves are notoriously robust against realistic zonal winds; unless there is a strong vertical wind shear near the equator, Kelvin waves are stable (Sakai 1989).

There has been no systematic understanding of the effect of the meridional/vertical circulation on these equatorially trapped waves, probably because this component of the circulation is, in an absolute sense, weaker than the zonal component. However, as we have argued, the strength of the background circulation has to be normalized to the direction of travel, and in that sense, the meridional circulation is as important as the zonal wind when studying planetary-scale equatorial waves. Furthermore, data show that the meridional wind convergence is equatorially confined in the lower troposphere, exactly where the equatorial waves have most of their power. This paper is a first attempt to understand the effect of meridional circulation on planetary-scale equatorial waves. To do so, we neglect the effect of zonal winds for two reasons. First and foremost, the effective zonal wind is concentrated in the subtropical jets, high in the troposphere and away from the equatorial Kelvin and Rossby waves, and its effects have been well studied (Wang and Xie 1996; Biello and Majda 2004). The results of these studies show that zonal winds cause synoptic-scale instabilities on the poleward ends of the subtropical jets and coupling of equatorial and midlatitude Rossby waves. Unless the subtropical jets are exceedingly strong and close to the equator, the equatorial Kelvin wave remains remarkably robust and stable against the zonal wind (Sakai 1989). Second, the well-studied instabilities associated with the zonal winds select for synoptic and smaller scales whereas the meridional circulation (as will be shown below) has its most

significant effect at the largest zonal length scales in the problem. In this paper we focus on planetary zonal length scales only.

In section 2 of this paper, the IMMD framework is used to derive a simplified set of equations describing the behavior of equatorial atmospheric waves in the presence of a planetary-scale overturning meridional–vertical circulation. A two-layer equatorial shallow-water system is constructed in the IMMD theory, the solutions of which—barotropic planetary Rossby waves, equatorially trapped, baroclinic Rossby waves, and Kelvin waves—do not interact in the absence of the background circulation but couple to each other in the presence of a meridional/vertical background flow.

We study the linear eigenvalue problem of the meridionally advected tropical long-wave theory in section 3. We show that the two-vertical-mode model, coupled through meridional advection, is skew self-adjoint; therefore all solutions are neutrally stable. This is in stark contrast to equatorial wave perturbations in the presence of zonal shear flow, where barotropic and baroclinic instabilities are common. We will also describe three novel effects of the meridional circulation on the classical Matsuno modes, First, by coupling to barotropic Rossby waves that have a significant midlatitude projection, the circulation creates a mechanism through which equatorial Rossby waves leak into midlatitude Rossby waves. Second, the Kelvin waves in the coupled model acquire a barotropic component. This barotropic component has easterly barotropic wind collocated with the maximum of the equatorial Kelvin wave's lower-tropospheric convergence, resulting in westward tilt with height of the Kelvin wave. Third, we will find that the meridional circulation causes a complete breakdown of the wave eigenfunctions of the lowest-frequency waves at the latitude where the background meridional flow vanishes. This feature, meridional convergence exceeding wave frequency, establishes a minimum frequency cutoff for linear equatorial Rossby and Kelvin waves in the presence of meridional circulation.

In section 4, we interpret our results in the context of observations and discuss future directions of study, especially including the subtropical jets and meridional circulation in the long-wave IMMD theory.

2. The model

a. IMMD

Majda and Klein (2003) used self-consistent, systematic asymptotic methods to develop the theory of intraseasonal planetary equatorial synoptic-scale dynamics, which describes large-scale atmospheric motions on two interacting spatial scales: synoptic and zonally long-wave planetary scales. The IPESD scales are appropriate to model planetary-scale dynamics coupled to synoptic-scale (Gill 1980) dynamics. Biello and Majda (2010) extend IPESD in their IMMD theory to allow for stronger mean heating on planetary scales, sufficient to drive a Hadley cell.

The derivation of IMMD begins with nondimensionalizing the variables and scales of the equatorial primitive equations appropriate to tropospheric conditions. The Coriolis force is a linear function of distance from the equator with constant of proportionality $\beta = 2\Omega R^{-1} = 2.27 \times 10^{-11}\ \mathrm{m^{-1}\,s^{-1}}$ (where $R = 6400$ km is Earth's radius and $\Omega = 2\pi\ \mathrm{day}^{-1}$ is its frequency of rotation). The horizontal velocity variables are measured in units of the dry gravity wave speed $c = 50\ \mathrm{m\,s^{-1}}$, meridional lengths in units of the equatorial deformation radius $L_E = (c/\beta)^{1/2} \approx 1500$ km, and time in units of the synoptic time scale $T_E = (c\beta)^{-1/2} \approx 8.3$ h. The vertical height scale is the height of the tropical troposphere divided by π, $H_T/\pi \approx 5$ km. IMMD also makes use of a planetary zonal length scale $L_P = 10\,L_E \approx 15\,000$ km and intraseasonal time scale $T_I = 10\,T_E \approx 3.3$ days to study large-scale intraseasonal variations in the tropics, with mean heating rates on the planetary scale of $10\,\mathrm{K\,day^{-1}}$. In the present study, we focus on the planetary-scale waves evolving on the intraseasonal time scale.

In the IMMD theory, motions on planetary scales are described by the trade winds/Hadley (TH) equations. The large-scale flows are in hydrostatic and meridional geostrophic balance, and advective nonlinearity is as important as the linear Coriolis and stratification terms. The TH equations are the long-wave, nonlinear equatorial primitive equations

$$\frac{D}{Dt}U - yV + P_x = -\mathscr{D}, \tag{3a}$$

$$yU + P_y = 0, \tag{3b}$$

$$P_z = \Theta, \tag{3c}$$

$$\frac{D}{Dt}\Theta + W = H - \mathscr{R}, \tag{3d}$$

$$U_x + V_y + W_z = 0, \quad \text{and} \tag{3e}$$

$$\frac{D}{Dt} = \frac{\partial}{\partial t} + U\frac{\partial}{\partial x} + V\frac{\partial}{\partial y} + W\frac{\partial}{\partial z}, \tag{3f}$$

forced by diabatic heating H, momentum dissipation $\mathscr{D}$, and radiation $\mathscr{R}$, all of which are filtered on the largest scales. In this regime, the zonal U, meridional V, and vertical W velocities are measured in units of $50\,\mathrm{m\,s^{-1}}$, $5\,\mathrm{m\,s^{-1}}$, and $1.6\,\mathrm{cm\,s^{-1}}$, respectively. The potential temperature Θ and the Exner function P (like geopotential height or a scale pressure) are measured in units of 33 K and $2500\,\mathrm{m^2\,s^{-2}}$, respectively (Biello and Majda 2010). These magnitudes of the velocity field are

consistent with the subtropical (zonal) winds and the meridional component of the Hadley circulation. Despite describing a vector field whose zonal, meridional, and vertical components are of significantly different magnitudes, all three components of the velocity field are present in the advective derivative since the anisotropy in the zonal, meridional, and vertical derivatives' scaling is in inverse proportion to the zonal, meridional, and vertical velocity scaling, respectively.

IMMD separates the zonally long planetary-scale anomalies from the mean TH system. The equations for the anomalies are

$$\frac{D}{Dt}u + (uU)_x + (vU)_y + (wU)_z - yv + p_x = F^u, \quad (4a)$$

$$yu + p_y = 0, \quad (4b)$$

$$p_z = \theta, \quad (4c)$$

$$\frac{D}{Dt}\theta + w + (u\Theta)_x + (v\Theta)_y + (w\Theta)_z = F^\theta, \quad \text{and} \quad (4d)$$

$$u_x + v_y + w_z = 0. \quad (4e)$$

The planetary-scale zonal u, meridional v, and vertical w wind anomalies are measured in units of 5, 0.5, and 0.16 m s^{-1}, respectively—which is an order of magnitude less than the mean flows. The zonal momentum and the potential temperature of the planetary-scale fluctuations are advected by the climatology (the TH velocities) and forced by upscale fluxes of zonal momentum F^U and temperature F^θ from the synoptic scales.

The IMMD theory closes the system of equations for the synoptic-scale fluctuations thereby providing an explicit expression for the upscale fluxes. Since this paper will not deal with the synoptic-scale fluctuations, the reader is referred to Biello and Majda (2010) for a description of the synoptic-scale theory. Briefly, the synoptic-scale theory consists of Matsuno's linear equations in the presence of zonal wind, forced by diabatic heating, but not damped in the manner of Gill (1980).

In the multiscale models of the MJO (Biello and Majda 2004), the planetary-scale organized flow exists as a packet of modulated synoptic-scale activity and, as such, is described by the equations of the planetary-scale anomalies [Eqs. (4)]. In the original multiple scale theory, the envelope was envisioned as a planetary-scale perturbation of a zero flow background state forced by the upscale fluxes. However, in the derivation of IMMD (Biello and Majda 2010) it was noted that a nontrivial background state could have significant implications for the initiation and propagation of the MJO. It is this question, the initiation and evolution of planetary-scale anomalies in the presence of a meridional overturning circulation, which motivates this study.

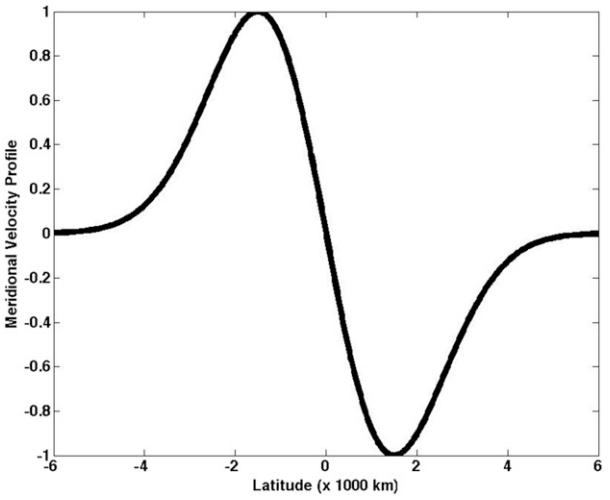

FIG. 2. Meridional profile of the meridional velocity $V(y)$ with maximum amplitude of 1 m s^{-1}. The examples in this paper use $L = 1$, which corresponds to the maximum meridional velocity occurring at 1500 km north or south of the equator. This flow is chosen so that it is convergent in the lower troposphere at the equator (and ascending there) and descends poleward of 1500 km from the equator.

b. *Planetary-scale anomalies with overturning circulation*

Mean zonal winds near the equator are much smaller than the 50 m s^{-1} that is described by the IMMD theory, yet mean meridional velocities are on the order of 2–3 m s^{-1} there (see Fig. 2). An asymptotic theory like IMMD sets an *upper* limit on the strength of the flow that it can describe. This means that flows of $|U| \approx 1$ (i.e., 50 m s^{-1}) can be consistently described by IMMD. However, the observational result we exploit throughout this paper is that equatorial winds are much smaller than 50 m s^{-1} (more like a few meters per second), so that the U term in IMMD can be safely discarded when considering the longest equatorially confined waves. Effectively, $|U| < 0.1$, but $|V| \approx 0.6$ near the equator; therefore it is an acceptable first approximation to neglect the zonal velocity when considering the meridional convergence effects near the equator. To study the effect of an overturning meridional and vertical background flow, especially near the equator, the zonal flow U is neglected in the equations governing the climatology [Eqs. (3)], and the remaining variables are assumed to be constant in time and in the zonal direction. The pressure variation P of the IMMD is driven by the zonal wind through geostrophic balance and is itself an anomaly from the atmosphere's mean pressure profile. Requiring $U = 0$ thus yields $P = 0$. It further follows from hydrostatic balance that the potential temperature variation Θ must also be zero. The meridional and vertical wind can then be modeled by the incompressibility constraint alone,

$$V_y + W_z = 0, \tag{5a}$$

along with the weak temperature gradient approximation

$$W = H - \mathscr{R} \equiv S^\theta, \tag{5b}$$

in which large-scale uplift W is proportional to the net heating rate S^θ.

In the equations of planetary-scale anomalies [Eqs. (4)], imposing $U = \Theta = 0$ and neglecting the upscale fluxes yields the zonally long-wave, incompressible, hydrostatic, linear equatorial primitive equations advected by the meridionally overturning background flow:

$$u_t + Vu_y + Wu_z - yv + p_x = 0, \tag{6a}$$
$$yu + p_y = 0, \tag{6b}$$
$$p_z = \theta, \tag{6c}$$
$$u_x + v_y + w_z = 0, \quad \text{and} \tag{6d}$$
$$\theta_t + V\theta_y + W\theta_z + w = 0. \tag{6e}$$

This is the long-wave Matsuno theory on a meridional background circulation governed by the weak temperature gradient with zonally symmetric heating, and it conserves a positive definite form of energy, specifically

$$\frac{\partial}{\partial t}\left[\frac{1}{2}(u^2 + \theta^2)\right] + \nabla \cdot \left[\frac{1}{2}(u^2 + \theta^2)\mathbf{U} + p\mathbf{u}\right] = 0, \tag{7}$$

where $\mathbf{U} = V\mathbf{j} + W\mathbf{k}$.

c. Two-layer model

The three-dimensional system of planetary-scale anomalies in the presence of an overturning meridional–vertical background circulation [Eq. (6)] can be projected onto a two-layer model in the vertical [similar to the two-level method applied by Wang and Xie (1996) and equivalent to the Galerkin truncation of Majda and Biello (2003)], yielding coupled systems of shallow-water equations,

$$\partial_t u_1 - yv_1 + \partial_x p_1 = -V\partial_y u_0, \tag{8a}$$
$$yu_1 + \partial_y p_1 = 0, \tag{8b}$$
$$\partial_x u_1 + \partial_y v_1 + \partial_t p_1 = 0, \tag{8c}$$
$$\partial_t u_0 - yv_0 + \partial_x p_0 = -\partial_y (Vu_1), \tag{8d}$$
$$yu_0 + \partial_y p_0 = 0, \quad \text{and} \tag{8e}$$
$$\partial_x u_0 + \partial_y v_0 = 0, \tag{8f}$$

where the 0 subscripts indicate the barotropic fields and the 1 subscripts the baroclinic fields. In projecting onto vertical modes, the variable W has been eliminated via the incompressibility constraint [Eq. (5a)]. The projection is presented in appendix A.

When the background circulation, now wholly represented by V in Eqs. (8a) and (8d), is omitted, the baroclinic and barotropic systems decouple; the decoupled baroclinic solutions are the classical long-wave Matsuno modes, while the barotropic component describes Rossby waves.

Conservation of energy as in Eq. (7) is retained in the projection, since

$$\frac{\partial}{\partial t}\left[\frac{1}{2}(u_0^2 + u_1^2 + p_1^2)\right] + \nabla \cdot (\mathbf{u}_0 p_0 + \mathbf{u}_1 p_1) + \frac{\partial}{\partial y}(Vu_0 u_1) = 0. \tag{9}$$

The energy density is always positive, so solutions remain neutrally stable.

d. Generalized eigenvalue problem

Since the coefficients of Eqs. (6) and (8) are constant in time and in the zonal direction, normal modes of the form $u_0(x, y, t) = \hat{u}_0(y)\, e^{ik(x-ct)}$ constitute the eigenfunctions of the system. By specifying the wavenumber k, the phase speed c is determined as an eigenvalue of the system

$$V\partial_y \hat{u}_0 - y\hat{v}_1 + ik\hat{p}_1 = ikc\hat{u}_1, \tag{10a}$$
$$y\hat{u}_1 + \partial_y \hat{p}_1 = 0, \tag{10b}$$
$$ik\hat{u}_1 + \partial_y \hat{v}_1 = ikc\hat{p}_1, \tag{10c}$$
$$\partial_y(V\hat{u}_1) - y\hat{v}_0 + ik\hat{p}_0 = ikc\hat{u}_0, \tag{10d}$$
$$y\hat{u}_0 + \partial_y \hat{p}_0 = 0, \quad \text{and} \tag{10e}$$
$$ik\hat{u}_0 + \partial_y \hat{v}_0 = 0, \tag{10f}$$

for the two-layer model. Beginning in section 3, to ease the notation, we will drop the hats on top of the variables when discussing the eigenfunctions. Neutral stability has been retained in the projection onto Fourier modes in x and t, so the eigenvalues c of the system of projected equations [Eqs. (10)] are real.

e. Overturning background circulation

To study the zonally long anomalies in the presence of a background flow resembling the meridional and vertical components of a zonally symmetric, temporally invariant Hadley cell, we consider planetary-scale heating of the form

$$S^\theta = -\frac{V_{\max}}{L}\left(1 - \frac{y^2}{L^2}\right)\exp\left(\frac{L^2 - y^2}{2L^2}\right)\sin(z), \tag{11}$$

where the parameter $V_{\max}$ controls the strength of the background circulation, and L controls the width of the

overturning cell. As dictated by Eqs. (5a) and (5b), this heating drives the meridional/vertical circulation:

$$\begin{bmatrix} V \\ W \end{bmatrix} = -\frac{V_{\max}}{L} \exp\left(\frac{L^2 - y^2}{2L^2}\right) \begin{bmatrix} y \cos z \\ (1 - y^2/L^2) \sin z \end{bmatrix}. \quad (12)$$

In the two-layer model, the background flow is represented by the meridional component,

$$V_1 = -\frac{V_{\max}}{L} y \exp\left(\frac{L^2 - y^2}{2L^2}\right), \quad (13)$$

since the vertical component is determined through incompressibility. This circulation rises within $|y| < L$ of the equator and descends poleward of this latitude. The meridional profile of the meridional velocity is shown in Fig. 2, for the parameters $L = 1$ corresponding to 1500 km and $V_{\max} = 1\,\mathrm{m\,s^{-1}}$. It is clear that this meridional velocity profile reaches its maximum at $y = L$, converges at the equator, and attains a maximum convergence of $V_{\max}/L$. Off-equatorial ITCZs may be important for teleconnections (Liu and Wang 2013), but the consideration of more general profiles will be left for future work.

All figures herein were produced by a background circulation of precisely this form, with $L = 1$, but with varying strengths of circulation. However, many of the conclusions presented herein apply for much more general background circulations; details of the precise restrictions that lead to the various results accompany the results themselves. Since the meridional component of the background flow has no projection onto the barotropic mode, the subscript 1 is elsewhere suppressed.

f. Numerical method and boundary conditions

Equations (10a)–(10f) constitute an eigenvalue problem for the wave speed c and eigenfunctions $(\hat{u}_0, \hat{v}_0, \hat{p}_0, \hat{u}_1, \hat{v}_1, \hat{p}_1)$. The linear operator is a nonconstant coefficient differential operator in y, that is, it contains derivatives with respect to y as well as the prespecified function $V(y)$.

At first glance there are three parameters in this eigenvalue problem: $V_{\max}$, L, and the zonal wavenumber k. In fact, the parameters reduce to two since the eigenvalue problem can be recast in terms of $V_{\max}/k$; this greatly reduces the size of the parameter space that we have to study. Although it is not computationally necessary to make this rescaling, the interpretation of the results of this rescaling are illuminating, so we present it in appendix B.

When $V_{\max} = 0$ the solutions of the baroclinic and barotropic problems decouple. The baroclinic solutions are the equatorially confined Kelvin wave (eigenvalue 1) and the long Rossby waves (negative eigenvalues) (Biello and Majda 2004). The barotropic solutions are sinusoidal in y, and all have negative eigenvalues. On a beta plane of infinite length, the barotropic solutions' eigenvalues consist of a continuous spectrum: any real number less than zero. On a finite domain the eigenvalues and corresponding eigenmodes are countably infinite with an accumulation point only at $c = 0$.

We extend the equatorial β plane far beyond its region of validity, to 16 500 km north and south of the equator. On this domain, we choose a basis of sines and cosines and project the primitive equations onto this basis. For the computations shown in this paper we use 2^{12} equally spaced collocation points to perform the integrations associated with the projection. We decreased the number of points down to 2^9 and did not find a noticeable difference in the eigenvalues or eigenfunctions. After projection there results a large but sparse matrix whose eigenvalues are the wave speeds c and whose eigenvalues are the Fourier series coefficients of the eigenfunctions. This is easily inverted in Matlab.

By using a Fourier series representation of the equations, we are effectively periodizing the β plane. However, if the eigenfunctions are localized away from the jump discontinuity in the Coriolis parameter at $y = \pm 16\,500$ km, then the Fourier convergence theorem guarantees that the numerically calculated solutions converge to the actual solutions in the limit of infinite collocation points. This explains the choice of extremely large meridional extent, which ensures that the effects of periodizing the problem are not felt by the equatorially trapped eigenfunctions. We will find that, for negative waves speeds, the barotropic components of the eigenfunctions are not localized near the equator. This, too, does not pose a problem for the convergence of the spectral numerical method since we expect barotropic modes to not be equatorially confined. We confirm that the baroclinic components of these coupled eigenfunctions are always equatorially confined.

One final technical detail follows. The spectrum of the uncoupled baroclinic modes is known to be $c = 1, -1/3, -1/5, \ldots$ etc., with all the negative odd integers in the denominators. These are the Kelvin wave and the long equatorial Rossby waves traveling at speeds $50, 50/3 = 16.66, 50/5 = 10, \ldots\ \mathrm{m\,s^{-1}}$. The spectrum of the uncoupled barotropic problem is doubly degenerate with eigenvalues $c = D/\pi n$, where D is the poleward extent of the domain in units of the equatorial deformation radius $D = 16\,500/1500 = 11$ and n is a positive integer. We have chosen D to ensure that there is not an exact resonance between the uncoupled barotropic waves and the lowest few baroclinic waves. This avoids any spurious solutions that are an artifact of the periodization and would not occur on Earth.

3. Results

a. Stability

In a midlatitude context, Rayleigh (1880) considers instabilities in meridionally sheared zonal flow; Charney (1947) and Eady (1949) study the conversion of mean-flow available potential energy into growing disturbances for a vertically sheared zonal flow. Xie and Wang (1996) investigate baroclinic instability in the equatorial context. While all of these studies demonstrate that sheared zonal background flow produces instabilities in its perturbation flows, it transpires that the same is not true of purely meridional and vertical background flows that obey the three-dimensional incompressibility constraint. An immediate consequence of requiring that the zonal flow component of the climatology [Eq. (3)] and the upscale fluxes be identically zero is the neutral stability of the resulting system of zonally long anomalies [Eq. (6)]; the energetics [Eqs. (7) and (9)] admit only solutions that are periodic zonally and temporally. As a result, given a real wavenumber k, Eqs. (10) for wave speed and amplitude admit only real speeds c.

b. Critical layers

When $V(y) = 0$ everywhere, the baroclinic and barotropic ODEs are second order in y. In fact, in the absence of V, Eqs. (10) do not contain any derivatives of $u_{0,1}$ with respect to y. The introduction of $V(y) \neq 0$ also introduces derivatives of $u_{0,1}$ with respect to y; the derivatives are multiplied by $V(y)$. The coupled system is not a fourth-order system (the sum of the two second-order systems) but rather a sixth-order system of ODEs. This makes it a singular perturbation because two new solutions appear. However, the sixth-order system has an additional peculiarity: there is a latitude y_* where $V(y_*) = 0$ and, therefore, the coefficient of the highest derivative vanishes at this latitude (in our examples, this will always be the equator). ODEs in which the coefficient of the highest-order term vanishes at some $y = y_*$ are well known to have singular solutions (i.e., solutions that diverge at $y = y_*$).

These types of singular solutions constitute the continuous spectrum in Rayleigh's equation for inviscid zonal shear flow and create the well-known critical layers in those flows. For barotropic zonal shear flows, these layers are neutrally stable and occur where the wave speed matches the flow speed. The eigenfunctions of these critical layers can have a discontinuous derivative.

To capture the essence of these critical layers in the meridionally sheared equatorial wave equations, we recognize the fact that a singular perturbation with a vanishing highest-order coefficient has the possibility of an eigenfunction with a singularity at $y = y_*$. We remind the reader that a function that blows up at y_* (a singular function) has derivatives that blow up even faster (they are more singular). To find the dominant balance of terms that capture this singularity we must ask, when looking at singular solutions, which of $(u_0, v_0, p_0, u_1, v_1, p_1)$ diverges the most near y_*?

If we hypothesize that v_0 is singular, then barotropic incompressibility [Eq. (8f)] demands that u_0 be more singular. Similarly if we hypothesize that p_0 is singular, then zonal geostrophic balance of the barotropic flow [Eq. (8e)] demands that u_0 be more singular. Therefore u_0 is more singular than v_0 and p_0; these latter two are regular near y_*, but have singular derivatives according to the geostrophic and incompressibility constraints. Therefore, in the vicinity of y_* we can neglect v_0 and p_0 in the barotropic momentum equation [Eq. (8d)]. The same arguments apply to the baroclinic equation, so we can neglect v_1 and p_1 in Eq. (8a).

Therefore, in the two-layer eigenproblem [Eq. (10)], in a neighborhood about the vanishing latitude y_*, the dominant terms are

$$V\partial_y u_0 = ikcu_1 \quad \text{and} \tag{14a}$$

$$\partial_y(Vu_1) = ikcu_0 \tag{14b}$$

[recall the comment after Eq. (10) that we have dropped the hats on the variables to lighten the notation]. This system can be reduced to a single second-order equation in either of its unknowns, for example,

$$V^2 u_{0yy} + 2VV_y u_{0y} + \omega^2 u_0 = 0, \tag{15}$$

where $\omega = ck$ denotes frequency. If we assume V vanishes linearly [$V \approx \alpha(y - y_*)$, which is the generic case], then Eq. (15) takes the form of Euler's differential equation,

$$\tilde{y}^2 u_{0\tilde{y}\tilde{y}} + 2\tilde{y}u_{0\tilde{y}} + \frac{\omega^2}{\alpha^2}u_0 = 0, \tag{16}$$

where we have defined $\tilde{y} = y - y_*$, and whence solutions are found to be proportional to

$$u_0 = \tilde{y}^{-1/2 \pm \sqrt{1/4 - (\omega/\alpha)^2}}, \tag{17}$$

(and similarly for u_1). When the discriminant is nonnegative, in other words when $|\omega| \geq |\alpha|/2$, the family of solutions asymptotically approaches infinity at $y = y_*$, and an arbitrary solution within the layer, matched to an outer solution, will have unbounded energetics at the singularity. Solutions with a negative discriminant also have unbounded energy but oscillate rapidly as they diverge, more slowly, toward infinity; these solutions

have nearly finite energy, and thus the change of sign of the discriminant represents a transition between better- and worse-behaved solutions.

Put succinctly, physically viable eigenfunctions satisfy the condition that the magnitude of their frequency exceeds half the meridional convergence of the flow,

$$|\omega| > \frac{1}{2}\left|\frac{\partial V}{\partial y}(y_*)\right|, \tag{18}$$

at each y_*. The range of infeasible frequencies increases with increasing strength of the background flow. We emphasize that the cases we are focusing on are generic, in the sense that we have assumed that the meridional velocity of the background flow does not vanish at the same latitude where the meridional convergence vanishes. Flows where the meridional velocity and convergence vanish at the same latitude would satisfy a different Euler-type equation than Eq. (16) and therefore have a different behavior than Eq. (17).

The eagle-eyed reader has noticed by this point that the dominant terms on display in Eq. (14) are just the projection onto the vertical bases of the terms

$$u_t + Vu_y + Wu_z = 0. \tag{19}$$

While the precise nature of the cutoff [Eq. (18)] discussed herein is a function of the vertical truncation, it is more generally the case that near latitudes where the meridional convergence of the meridional background flow is strongest, or equivalently where vertical background flow is maximized, the system is characterized by advection and does not resemble Matsuno's equations. Thus the traditional equatorial wave profiles are destroyed by sufficiently strong background flow, with the lower-frequency waves being most affected. The implications of low-frequency wave cutoff are addressed in section 4.

c. *Global barotropic response for baroclinic Rossby waves*

In the presence of overturning flows whose amplitudes align with observations (less than $5\,\mathrm{m\,s^{-1}}$ zonally averaged meridional velocities), the zonally long perturbed flows' projections onto the first baroclinic mode closely resemble the classic long-wave Matsuno modes: equatorially trapped Kelvin and Rossby waves. The baroclinic Rossby waves remain equatorially trapped as in the classical theory and are coupled to barotropic plane waves by the overturning background circulation.

Figure 3 shows the amplitudes of the horizontal velocity fields for the classical Matsuno Rossby wave and for the analogous wave in the presence of a moderate overturning background circulation. The background circulation has negligible effect on the baroclinic component of the wave, which remains equatorially trapped. However, a global barotropic response is induced (dashed lines in Figs. 3b,d). Outside the tropics, both the zonal and meridional barotropic winds vary sinusoidally; at the equator the zonal velocity and the meridional velocity's y derivative exhibit a global maximum in magnitude (for waves having opposite parity about the equator, such as the second-gravest baroclinic Rossby wave, these statements are reversed).

The horizontal wind fields corresponding to Fig. 3 are plotted in the upper and lower troposphere in Fig. 4. In the absence of background flow (Figs. 4b,d), the Rossby wave's wind field lacks horizontal tilt. In the presence of moderate overturning background flow (Figs. 4b,d) the wind fields tilt eastward and poleward in the upper troposphere and westward and poleward in the lower troposphere. The center of lower-tropospheric convergence (asterisks in Figs. 4c,d), which coincides with the longitude of vanishing zonal wind in the absence of background flow, is shifted into a region of equatorial lower-tropospheric easterlies by the overturning circulation.

We do not present the results in this paper, but argue that it is clear that the ratio of the barotropic to the baroclinic component of the eigenfunction increases with increased coupling strength. The coupling strength is proportional the maximum amplitude of the meridional circulation $V_{\max}$, inversely proportional to the latitude of its maximum L, and proportional to the zonal wavelength of the perturbation ($\propto k^{-1}$). For increasing coupling strength, this mode, which was originally the equatorially trapped Rossby wave, gains such a significant barotropic component and loses its baroclinic Rossby structure that it is no longer identifiable as a Matsuno Rossby wave; effectively, the meridional circulation shears the wave out of existence.

In general, a background circulation with first-baroclinic vertical structure produces wave–wave coupling between all consecutive vertical modes of perturbation flows. In the two-layer study coupling takes place between the barotropic and first-baroclinic modes. A similar coupling, between the baroclinic equatorial Rossby waves and the global (mostly extratropical) barotropic Rossby wave is known to occur in the presence of vertically sheared zonal flows In a similar two-level model, Wang and Xie (1996) find that while meridionally sheared zonal flows leave different vertical modes uncoupled, vertically sheared zonal flows produce coupling between the equatorial baroclinic Rossby waves and global barotropic waves. Majda and Biello (2003) and Biello and Majda (2004) demonstrate such a result for zonally long waves and derived a weakly nonlinear theory for tropical–extratropical Rossby interactions.

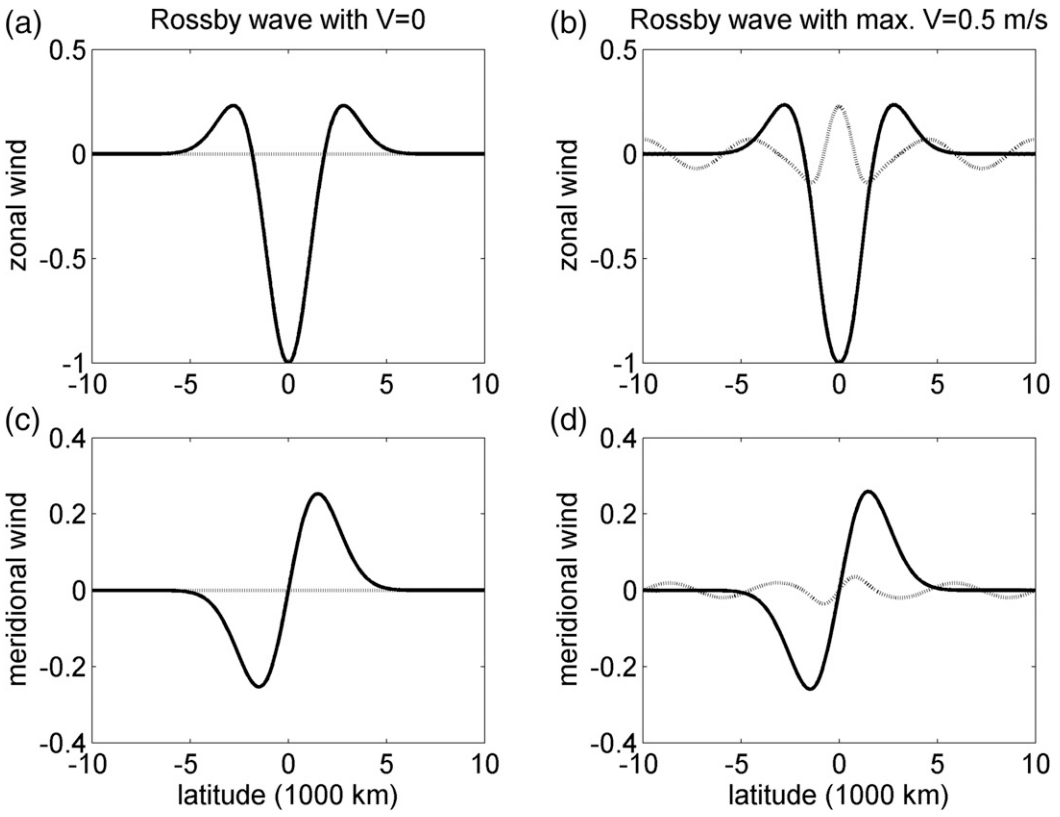

FIG. 3. Horizontal wind amplitudes of the gravest baroclinic Rossby wave of zonal wavenumber 2 (a),(c) without background circulation and (b),(d) in the presence of background circulation with maximum meridional velocity of 0.5 m s^{-1}, showing the (top) zonal and (bottom) meridional velocity component of the waves. Solid lines indicate baroclinic components while dashed lines indicate barotropic components. The zonal and meridional components are not in phase; the lower-tropospheric baroclinic zonal and barotropic meridional winds attain the amplitudes depicted 5000 km (1/4 period) east of the longitude where the lower-tropospheric baroclinic meridional and barotropic zonal winds attain the depicted amplitudes.

Although the detailed sinusoidal structure of the barotropic component of the wave as it approaches the poles is a consequence of the global beta-plane approximation, in spherical geometry such waves are still expected to escape the tropical waveguide. Therefore, these results show that through the meridional circulation the global barotropic plane wave component acts as a conduit of Rossby wave energy between the tropics and the extratropics. We leave to future work the additional effect of a zonal background flow, but results akin to those of Wang and Xie (1996) suggest that the critical layer associated with a vertically sheared zonal flow does not prevent the barotropic component of the flow from penetrating to midlatitudes.

d. Kelvin waves tilted west with height

Figure 5 shows the amplitudes of a zonal wavenumber-2 Kelvin wave's horizontal wind in the absence of all background flow (Fig. 5a) and in the presence of an overturning circulation (zonal and meridional wind, Figs. 5b and 5c, respectively). In the presence of a moderate meridional circulation, the Kelvin wave acquires barotropic zonal and meridional wind components that are comparable in magnitude to the Rossby wave's barotropic wind response to a background circulation (see Fig. 3). However, while the overturning circulation endows westward-traveling Rossby waves with a global barotropic component, the same is not true for the eastward-propagating Kelvin wave; the barotropic component of the coupled Kelvin wave is equatorially trapped. This is a consequence of the fact that Rossby waves cannot propagate eastward in the midlatitudes in the absence of shear. Put in terms of the equations, we see that a coupled Kelvin wave has a positive (eastward) frequency, and the barotropic equatorial equations when solved with a positive frequency yield exponentially decaying solutions.

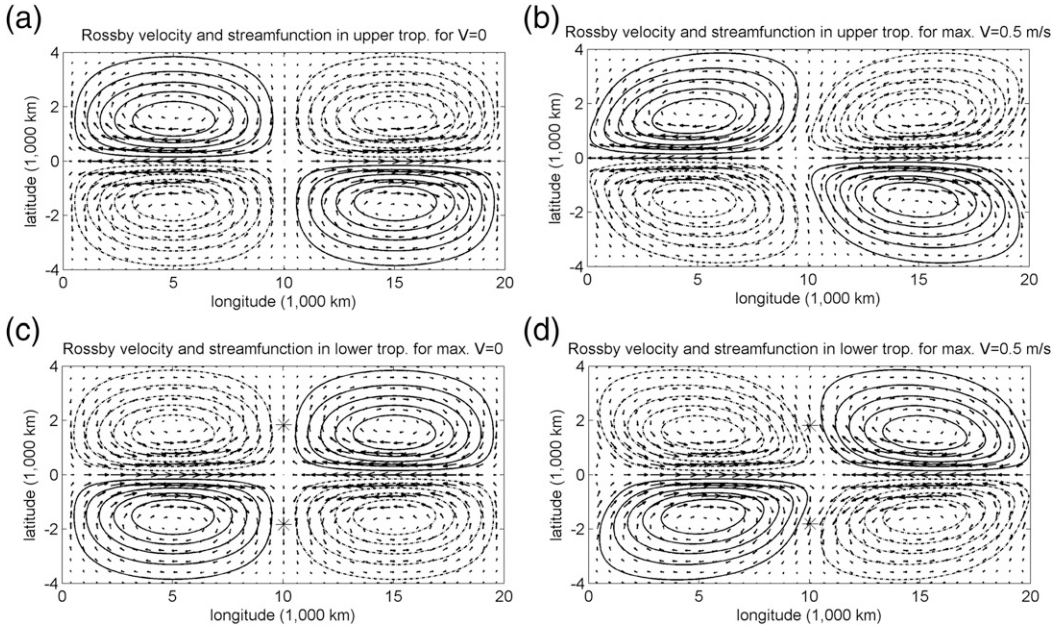

FIG. 4. Horizontal velocities and streamfunction in the (top) upper troposphere and (bottom) lower troposphere of a Rossby wave of zonal wavenumber 2. (a),(c) The Matsuno equatorial Rossby wave in the absence of background circulation; (b),(d) baroclinic/barotropic Rossby waves coupled by a background circulation with maximum meridional velocity $V = 0.5\ \mathrm{m\,s^{-1}}$. In (c) and (d), asterisks indicate the center of convergence.

The Kelvin wave's induced baroclinic meridional wind is a full order of magnitude smaller than its induced barotropic meridional wind. Investigating convectively coupled waves propagating along a symmetric ITCZ, Dias and Pauluis (2009) also find an induced meridional wind. However, the induced meridional wind in Dias and Pauluis (2009) increases with zonal wavenumber, since convective coupling plays a much larger role at small scales. The induced meridional wind in this paper increases with decreasing wavenumber since the meridional background circulation has the largest effect on the largest-scale waves.

Figure 6 shows the horizontal wind fields in the upper and lower troposphere for a Kelvin wave in the presence of a $3.5\ \mathrm{m\,s^{-1}}$ background circulation. The Kelvin wave in the absence of background flow is entirely first baroclinic, meaning that the wave displays neither eastward nor westward tilt with height (the nodal curve of zonal velocity is a vertical line), nor does it have a meridional component of velocity. When the overturning circulation is

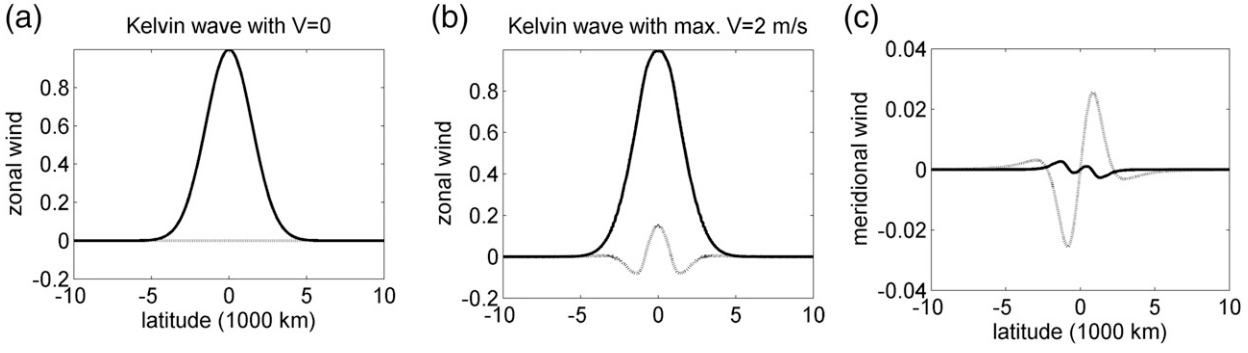

FIG. 5. Zonal wind amplitudes of the Kelvin wave of zonal wavenumber 2 (a) in the absence of background circulation and (b) in the presence of background circulation with maximum meridional velocity of $2\ \mathrm{m\,s^{-1}}$. Solid lines indicate baroclinic components while dashed lines indicate barotropic components. (c) The meridional velocity of the Kelvin wave in the presence of a $2\ \mathrm{m\,s^{-1}}$ meridional circulation [corresponding to the zonal velocity of (b)]. The uncoupled Kelvin wave in (a) carries no meridional velocity. The zonal and meridional velocities are not in phase; the lower-tropospheric baroclinic zonal and barotropic meridional winds attain the amplitudes depicted 5000 km (1/4 period) east of the longitude where the lower-tropospheric baroclinic meridional and barotropic zonal winds attain the depicted amplitudes.

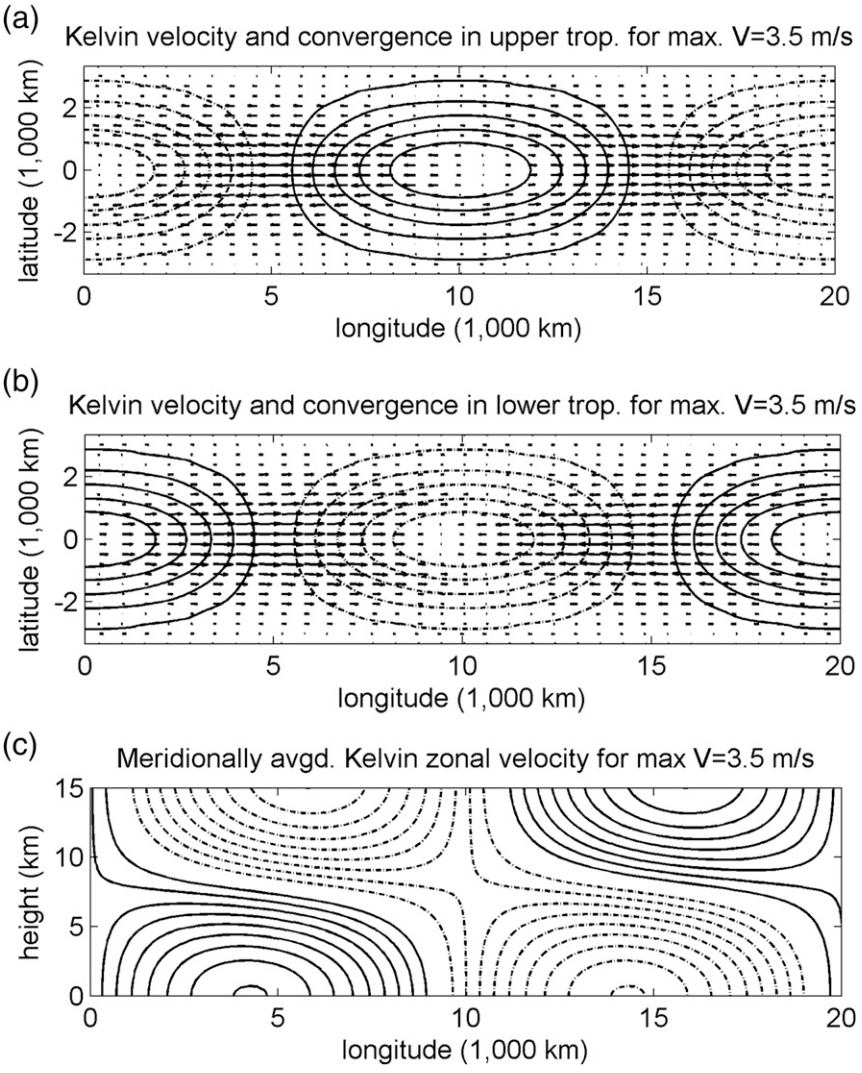

FIG. 6. Horizontal velocities and convergence in the (a) upper and (b) lower troposphere for a Kelvin wave of zonal wavenumber 2 in the presence of background circulation having maximum meridional velocity of 3.5 m s^{-1}. Solid (dashed) contours represent divergence (convergence). (c) The zonal velocity contours of the same Kelvin wave, meridionally averaged in the region within 1000 km of the equator. Solid (dashed) contours represent eastward (westward) flow.

introduced, and the Kelvin wave acquires a barotropic circulation, it also acquires a meridional velocity field and an unambiguously westward tilt with height. The induced barotropic component's maxima and minima lag those of the lower-tropospheric baroclinic wave, resulting in the eastward shift of the upper-tropospheric component relative to the lower. Since this shift is away from a purely first-baroclinic profile, the overall result is a westward tilt. In Fig. 6c the westward tilt with height of the zonal wind in the coupled Kelvin wave is evident. The tilt increases with increasing strength of background circulation (Fig. 6) and consequently, the coupled Kelvin wave acquires a zonal wind in the midtroposphere where, for a solely first-baroclinic Kelvin wave, there is none. The mid-tropospheric wind is westward above the maximum of lower-tropospheric convergence.

It is notable that the westward tilt coincides with that of observed convectively coupled Kelvin waves and in the waves embedded in the Madden–Julian oscillation (Kiladis et al. 2011; Zhang 2005). While we do not want to overstate the importance of this tilt, it does suggest a mechanism for the initiation of, and constructive feedback to, tilted (and therefore coherent) convective

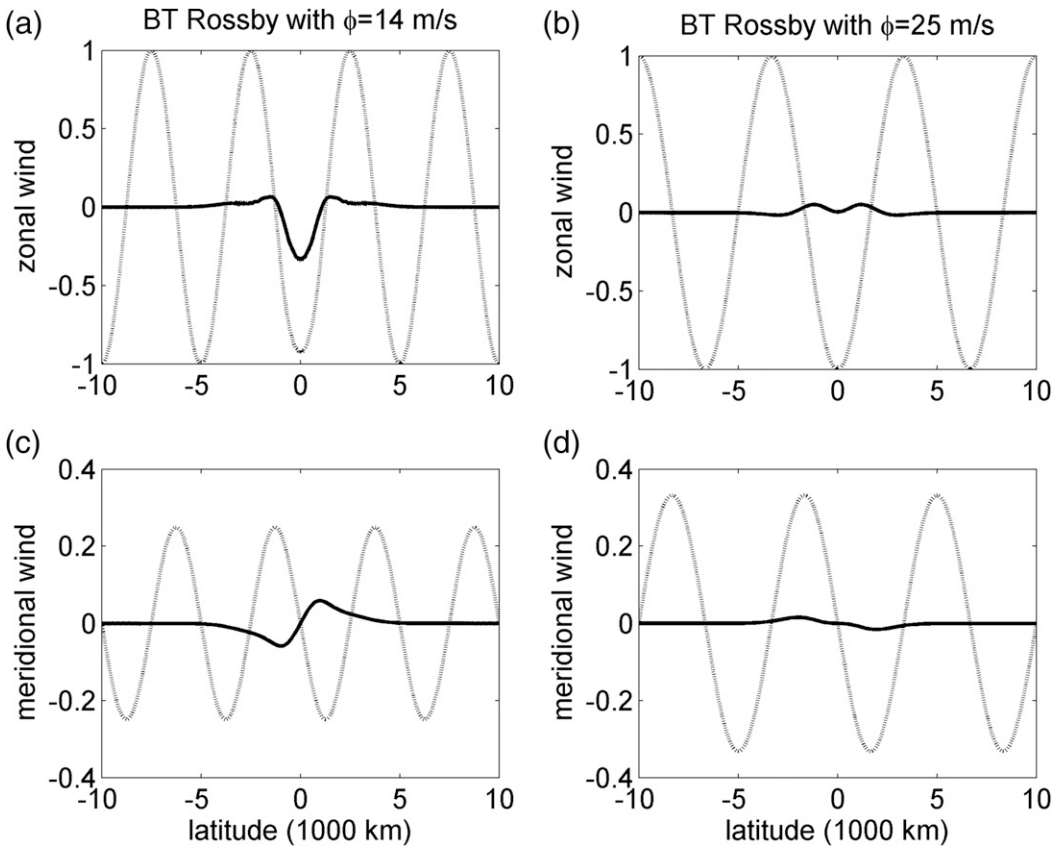

FIG. 7. Horizontal wind amplitudes of barotropic free Rossby waves of zonal wavenumber 2 in the presence of background circulation with maximum meridional velocity of 0.5 m s^{-1}. Since there is a continuous spectrum of barotropic Rossby waves, these panels show the waves whose wave speeds (eigenvalues) do not match the wave speeds of the equatorially trapped (Matsuno) Rossby waves; ϕ in the heading is the eigenvalue (wave speed) of each mode. Solid (dashed) lines indicate baroclinic (barotropic) components. (a),(c) Waves whose phase speed of 14 m s^{-1} falls within the range of the baroclinic Rossby waves' speeds; (b),(d) waves whose phase speed of 25 m s^{-1} is faster than all of the baroclinic Rossby waves, with results shown for the (top) zonal and (bottom) meridional components of the eigenfunctions. The various components are not in phase; the lower-tropospheric baroclinic zonal and barotropic meridional winds attain the amplitudes depicted 5000 km (1/4 period) east of the longitude where the lower-tropospheric baroclinic meridional and barotropic zonal winds attain the depicted amplitudes.

waves. It is also notable, albeit unphysical, that reversing the direction of the overturning circulation, so that air descends at the equator, results in an eastward tilt with height for the Kelvin wave. This may suggest that tropical ascent and westward tilt are inherent features of rotating, convective systems irrespective of the convective parameterization.

e. *Barotropic Rossby waves' equatorially trapped baroclinic response*

Figure 7 shows the amplitudes of the horizontal winds for two barotropic waves in the presence of the same background circulation. At left is plotted a wave whose wave speed (eigenvalue) does not match any baroclinic solutions to the decoupled equations but falls between two of them (it is nonresonant with a speed is 14 m s^{-1}, while two baroclinic Rossby waves have speeds of 16.67 and 10 m s^{-1}). At right is plotted a wave whose wave speed is higher than any zonally long westward-traveling baroclinic wave. The baroclinic response to the wave at left is an order of magnitude larger than the response to the wave at right. Additionally, the response to the wave at left is similar in meridional structure to a baroclinic Rossby wave of a similar frequency (the gravest baroclinic Rossby wave, as in Figs. 3a,c).

In the absence of background flow, the solutions to the barotropic portion of the two-layer model [Eqs. (8d)–(8f)] are westward-traveling barotropic plane waves. The effect of the overturning circulation is to produce an equatorially trapped baroclinic component

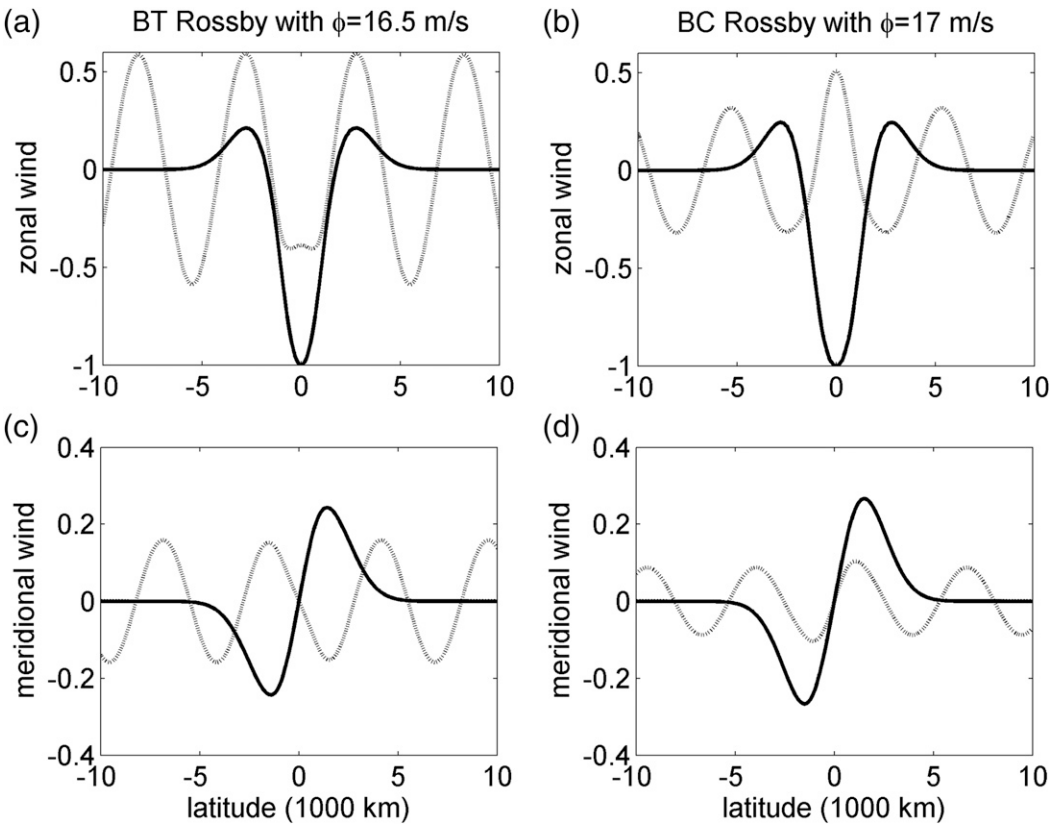

FIG. 8. Horizontal wind amplitudes of (a),(c) a barotropic free Rossby wave and (b),(d) a baroclinic Rossby wave with similar phase speeds; both have zonal wavenumber 2 and are in the presence of background circulation with maximum meridional velocity of 0.5 m s^{-1}. Since there is a continuous spectrum of barotropic Rossby waves, these panels show the waves whose wave speed is nearly resonant with the equatorially trapped Matsuno Rossby wave (which travels at 16.6 m s^{-1}); ϕ in the heading is the wave speed (eigenvalue) of each mode. Solid (dashed) lines indicate baroclinic (barotropic) components; results are shown for (top) zonal and (bottom) meridional components of the eigenfunctions. The various components are not in phase; the lower-tropospheric baroclinic zonal and barotropic meridional winds attain the amplitudes depicted 5000 km (1/4 period) east of the longitude where the lower-tropospheric baroclinic meridional and barotropic zonal winds attain the depicted amplitudes.

in these flows. Similar to the effect on baroclinic Rossby waves, the ratio of the amplitudes of baroclinic to barotropic components depends on wavenumber, on the strength of background circulation, and on the nearness in frequency of the uncoupled barotropic wave to any baroclinic Rossby wave; in particular, barotropic waves whose wave speed is faster than any baroclinic Rossby wave develop only small projections onto the baroclinic mode.

In the case of baroclinic and barotropic modes whose frequencies match or nearly match, the ratio between amplitudes of baroclinic and barotropic components is close to unity in the presence of moderate background circulation, and baroclinic and barotropic solutions appear similar to one another, with a relative phase shift between barotropic and baroclinic components. Figure 8 depicts a barotropic free Rossby wave (Figs. 8a,c) and a baroclinic equatorial Rossby wave (Figs. 8b,d) of similar phase speeds in the presence of moderate background circulation. Their baroclinic components are virtually identical; the barotropic components are distinguished by a phase shift of 180° and a moderate decrease in strength. The ratio of barotropic to baroclinic components is larger for the wave moving at the speed of an uncoupled, classical barotropic plane wave, although the barotropic components of the two waves are approximately the same strength.

The barotropic zonal component of the barotropic wave (Figs. 8a,c) is depressed at the equator while the barotropic zonal component of the baroclinic wave (Figs. 8b,d) attains its global maximum at the equator. The corresponding horizontal wind fields are plotted in the upper and lower troposphere in Fig. 9 (the barotropic wave) and Fig. 10 (the baroclinic wave). There is a

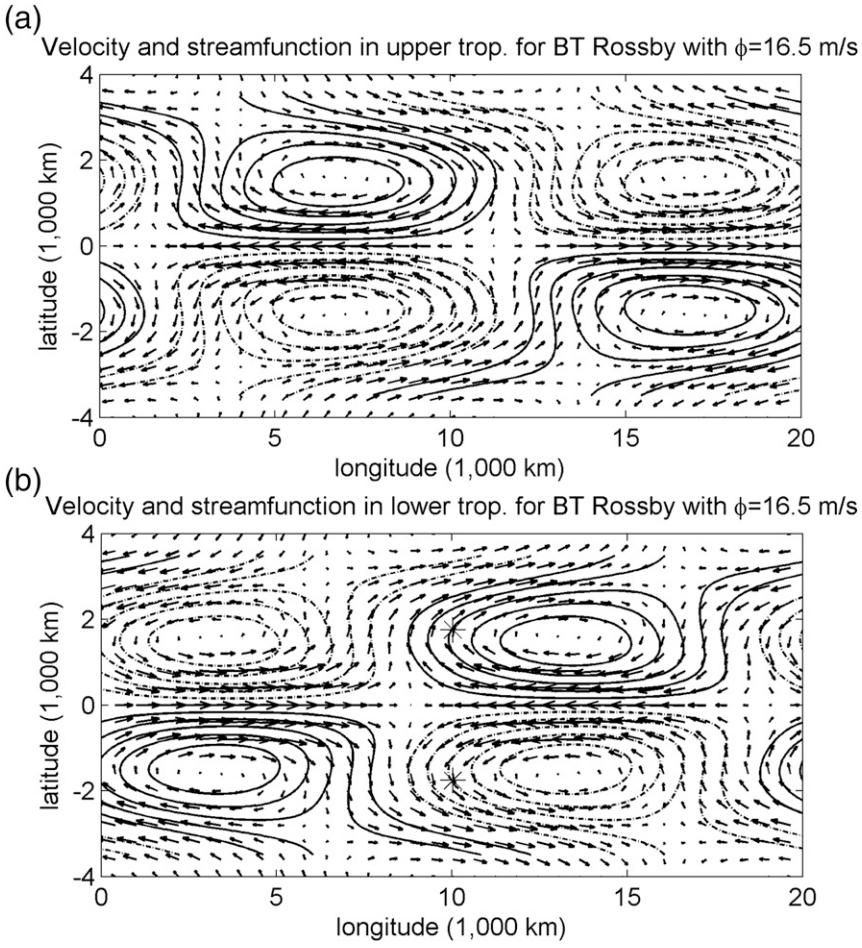

FIG. 9. Horizontal velocities and streamfunction in the (a) upper and (b) lower troposphere of a barotropic free Rossby wave of zonal wavenumber 2 with background circulation having maximum magnitude of meridional velocity $V = 0.5\ \mathrm{m\,s^{-1}}$. The meridional extent of the domain is such that the wave's frequency matches that of a baroclinic equatorial Rossby wave in the absence of background flow. In (b), asterisks indicate the center of convergence. Wind amplitudes are plotted in Figs. 8a and 8c.

distinct meridional inflow and outflow from the equatorial region corresponding to a meridional tilt, which itself is more pronounced in the baroclinic wave (Fig. 10).

4. Discussion

The IMMD theory is used to analyze zonally long waves on an equatorial beta plane in the presence of an overturning background circulation representing the meridional and vertical components of an idealized Hadley cell. In the resulting linear equations, the energy of the perturbation is both positive definite and conserved; therefore all eigenfunctions are neutrally stable. In a two-layer model, solutions are found to be modified baroclinic equatorial Rossby and Kelvin waves along with global barotropic plane waves. The overturning circulation produces coupling between the baroclinic waves and compatible barotropic components.

The equatorially trapped Rossby waves acquire a sinusoidal barotropic component that extends into the middle latitudes. The amplitude of the barotropic wind relative to the baroclinic wind increases with increasing magnitude of the background circulation, with an increasing zonal wavelength of the wave, and with the proximity of the baroclinic wave frequency (the eigenvalue) to that of a barotropic plane wave solution in the absence of background flow. In numerical studies, the inclusion of a realistic zonally averaged zonal flow did not prevent the barotropic component from extending to the midlatitudes.

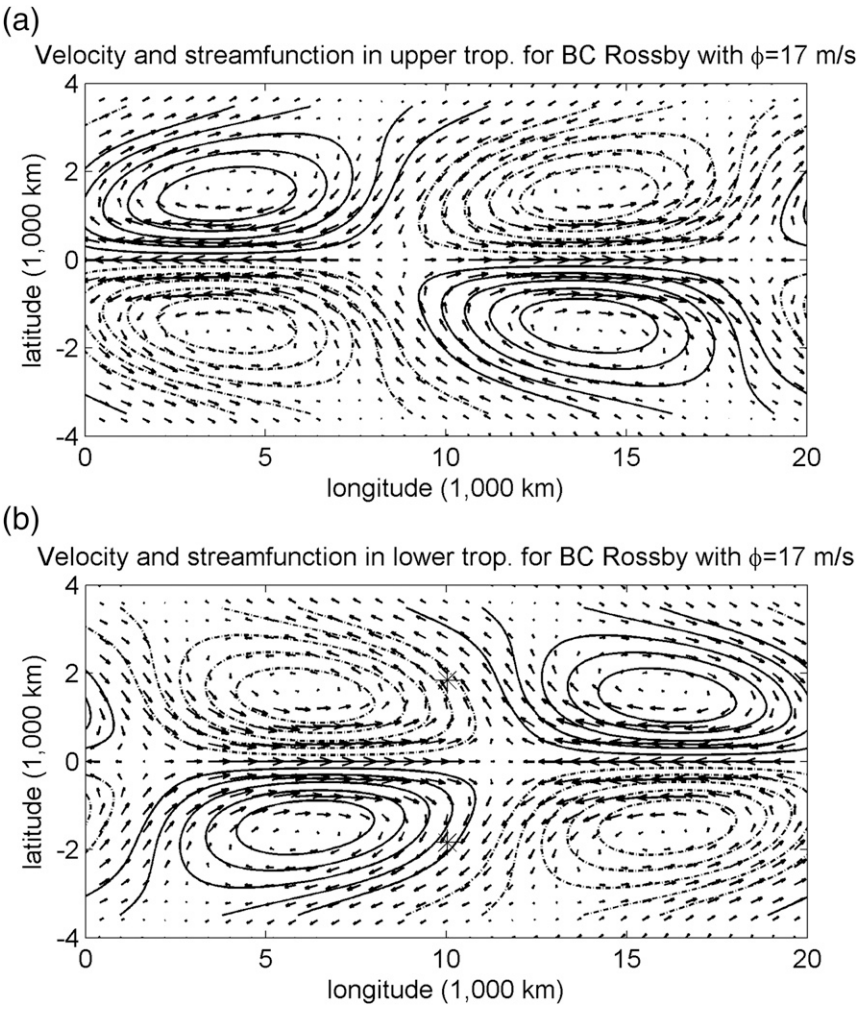

FIG. 10. As in Fig. 9, but for a baroclinic Rossby wave. The meridional extent of the domain is such that the wave's frequency matches that of a barotropic free Rossby wave in the absence of background flow. Wind amplitudes are plotted in Figs. 8b and 8d.

The Kelvin wave also acquires a barotropic component. However, its barotropic component is equatorially trapped and does not enable energy exchange with the extratropics. The most prominent effect of the Kelvin wave's coupling to its barotropic component is a westward tilt with height in the resulting zonal wind field. In numerical experiments, the Kelvin wave's vertical tilt is unaffected by the addition of a realistic zonal background flow.

In observations, equatorial Kelvin waves also exhibit westward tilt with height. Using space–time power spectra to isolate Kelvin wave signatures in radiosonde data, Kiladis et al. (2011) show westward-tilted zonal wind profiles for the wave above the island of Majuro; at the same location, Ogrosky and Stechmann (2016) identify the Kelvin wave by its theoretical eigenvector, including a first-baroclinic vertical structure, and find the same westward vertical tilt. Guo et al. (2014) study equatorial Kelvin waves over South America and the Atlantic Ocean, finding that the magnitude of vertical tilt varies during the various phases of the MJO, but is always westward with height. Many studies [including Mapes (2000)] have highlighted the role of the second baroclinic component of convection as a primary mechanism for creating tilt in equatorial waves. The result of this study does not contradict previous studies, but it provides an additional mechanism. That is to say, a meridional circulation that is generated by convection—convection whose zonal tilt is irrelevant because averaging on the planetary scales washes out any tilts—spontaneously creates westward tilts with height in the Kelvin waves that travel through it.

A minimum frequency cutoff for the existence of zonally long equatorial waves depends on the magnitude of the background flow's meridional convergence near latitudes where it vanishes. Whether waves in nature are subject to such a cutoff is unclear; space–time power spectra [as in Wheeler et al. (2000)] often display a gap between the lowest-frequency Kelvin wave and the MJO's signal, but for westward-propagating waves such a gap is not clear. On the other hand, when Ogrosky and Stechmann (2016) undertake to identify the gravest equatorial Rossby wave by its eigenfunction, the resulting power spectrum bears little resemblance to the theoretical dispersion relation. Therefore, it may be the case that part of the spectrum usually associated with Rossby waves actually corresponds to some other structures.

The relationship between the Kelvin wave's minimum frequency and the features of the background circulation is to be investigated in a future work as is the possible role played by the overturning background circulation in marshaling the transition between the MJO and Kelvin wave (Roundy and Kiladis 2006; Sobel and Kim 2012).

The main limitation of this study is the simplicity of the background profile, which is centered on the equator and invariant in time and space. In reality the Hadley cell varies in strength and space on seasonal time scales, and the observed planetary-scale meridional wind's projection onto zonal wavenumber 1 may exceed its zonally averaged strength. Incompressible meridional–vertical background flow is here shown to produce no growing long wave disturbances. However, Powell and Houze (2015) observe anomalous large-scale vertical motion leading the MJO events recorded by the DYNAMO field campaign. Therefore, some assumptions in this model will be relaxed to allow for background zonal variation in concert with destabilizing upscale fluxes, and a source of instability, particularly one leading to MJO initiation, sought therein. Additionally, the true Hadley cell's overturning circulation is coupled to a zonal component that is absent from this study. Investigation into the effects of a background flow that varies in space and time and has a nonzero zonal component is needed. Work is also underway to determine how upscale fluxes from the synoptic scales affect solutions; results will be reported elsewhere.

Acknowledgments. The authors thank George Kiladis for discussing realistic amplitudes of circulation, John Hunter for helping sort out the eigenfunctions of the coupled system, Fei Lui for forcing us to better explain the rationale for disregarding the zonal flow, and two anonymous referees for significantly helping improve the manuscript. Both authors were supported by the NSF under Grants DMS-1009959 and DMS-1313477.

APPENDIX A

Derivation of the Two-Layer Model

We now derive in detail the two-layer system [Eq. (8)] from the three-dimensional system of anomalies [Eq. (6)], which, according to Eq. (5a), can be rewritten as

$$u_t + (Vu)_y + (Wu)_z - yv + p_x = 0, \tag{A1a}$$

$$yu + p_y = 0, \tag{A1b}$$

$$p_z - \theta = 0, \tag{A1c}$$

$$u_x + v_y + w_z = 0, \quad \text{and} \tag{A1d}$$

$$\theta_t + (V\theta)_y + (W\theta)_z + w = 0. \tag{A1e}$$

We consider these equations over the domain $0 \le z \le \pi$. Define the characteristic functions

$$\chi_+ = \chi_{[\pi/2,\pi]}, \ \chi_- = \chi_{[0,\pi/2]}; \tag{A2}$$

then an orthogonal basis for a two-layer model is given by

$$\phi_0 = \chi_+ + \chi_- \quad \text{and} \tag{A3}$$

$$\phi_1 = \chi_- - \chi_+, \tag{A4}$$

(ϕ_0 describes the barotropic mode and ϕ_1 the baroclinic mode). Finally, define

$$\lambda(z) = \begin{cases} z, & z < \pi/2, \\ \pi - z, & z > \pi/2. \end{cases}$$

Then $d\lambda(z)/dz = \phi_1$.

We consider horizontal perturbation velocities u and v and pressure perturbations p projected onto the basis functions ϕ_0 and ϕ_1, while the vertical velocity w and potential temperature θ are projected onto α (note that this choice agrees with the vertical boundary conditions discussed in section 2f):

$$u = u_0(x,y,t)\phi_0(z) + u_1(x,y,t)\phi_1(z), \tag{A5a}$$

$$v = v_0(x,y,t)\phi_0(z) + v_1(x,y,t)\phi_1(z), \tag{A5b}$$

$$w = w_1(x,y,t)\lambda(z), \tag{A5c}$$

$$p = p_0(x,y,t)\phi_0(z) + p_1(x,y,t)\phi_1(z), \quad \text{and} \tag{A5d}$$

$$\theta = \theta_1(x,y,t)\lambda(z). \tag{A5e}$$

This is equivalent to the method of Wang and Xie (1996), who evaluate potential temperature and vertical

velocity at the midtroposphere and all other variables at both the middles of the upper and lower troposphere.

We also impose that the large-scale heating is proportional to α, so it is strongest at and symmetric about the middle troposphere; as a consequence, the vertical background velocity W is proportional to α, while the meridional background velocity is proportional to ϕ_1:

$$V = V_1(y)\phi_1(z) \quad \text{and} \tag{A6a}$$

$$W = W_1(y)\lambda(z). \tag{A6b}$$

The background incompressibility [Eq. (5a)] is then given by

$$V_{1y} + W_1 = 0, \tag{A7}$$

which is eventually used to eliminate W.

Projecting the anomaly equations for horizontal momentum [Eqs. (A1a) and (A1b)] and continuity [Eq. (A1d)] onto the barotropic basis function yields

$$u_{0t} + (V_1 u_1)_y - y v_0 + p_{0x} = 0, \tag{A8a}$$

$$y u_0 + p_{0y} = 0, \quad \text{and} \tag{A8b}$$

$$u_{0x} + v_{0y} = 0, \tag{A8c}$$

and projecting them onto the baroclinic basis function yields

$$u_{1t} + (V_1 u_0)_y + W_1 u_0 - y v_1 + p_{1x} = 0, \tag{A9a}$$

$$y u_1 + p_{1y} = 0, \quad \text{and} \tag{A9b}$$

$$u_{1x} + v_{1y} + w_1 = 0. \tag{A9c}$$

Projecting the remaining two equations onto $\lambda(z)$ produces

$$-p_1 = \theta_1 \quad \text{and} \tag{A10a}$$

$$\theta_{1t} + w_1 = 0, \tag{A10b}$$

which are used to eliminate w_1 from Eq. (A9c):

$$u_{1x} + v_{1y} + p_{1t} = 0. \tag{A11}$$

Background incompressibility [Eq. (A7)] is now used to eliminate the background vertical momentum from the baroclinic zonal momentum equation [Eq. (A9a)],

$$u_{1t} + (V_1 u_0)_y - V_{1y} u_0 - y v_1 + p_{1x} = 0, \tag{A12}$$

or, equivalently,

$$u_{1t} + V_1 u_{0y} - y v_1 + p_{1x} = 0. \tag{A13}$$

Finally, discarding the subscript 1 of the background meridional circulation yields the two-layer system [Eq. (8)].

APPENDIX B

Rescaling the Eigenvalue Problem

Define the new variables $(\tilde{u}_0, \tilde{v}_0, \tilde{p}_0, \tilde{u}_1, \tilde{v}_1, \tilde{p}_1) = (-i\hat{u}_0, -k^{-1}\hat{v}_0, -i\hat{p}_0, \hat{u}_1, -ik^{-1}\hat{v}_1, \hat{p}_1)$. The rescaled baroclinic zonal velocity and pressure are the same as the original zonal velocity and pressure. The barotropic zonal velocity and pressure are rescaled by a factor of $-i$, which corresponds to a quarter-period phase shift in the zonal direction. Therefore, all the eigenfunctions will have barotropic and baroclinic zonal wind and pressure components that are shifted by a quarter period from one another. The baroclinic meridional velocity is also rescaled by a factor of $-i$, so it will be shifted by a quarter period from the baroclinic zonal velocity; this is expected from the two components of the velocity field of a stable wave. The barotropic meridional velocity is shifted by a quarter period from the barotropic zonal velocity; again, this is expected from the two components of the velocity field of a stable wave. The last aspect of the rescaling is that both meridional components of the velocity are rescaled by k. This is exactly the scaling of the meridional velocity that occurs in the long-wave approximation of the equatorial waves. It is a consequence of the fact that for meridionally trapped waves (like equatorial Rossby waves), the meridional component of the velocity fields becomes weaker as the zonal wavelength increases (Majda and Biello 2003). The eigenvalue problem in the rescaled variables is

$$\left(\frac{V}{k}\right)\partial_y \tilde{u}_0 - y\tilde{v}_1 + \tilde{p}_1 = c\tilde{u}_1, \tag{B1a}$$

$$y\tilde{u}_1 + \partial_y \tilde{p}_1 = 0, \tag{B1b}$$

$$\tilde{u}_1 + \partial_y \tilde{v}_1 = c\tilde{p}_1, \tag{B1c}$$

$$-\partial_y\left[\left(\frac{V}{k}\right)\tilde{u}_1\right] - y\tilde{v}_0 + \tilde{p}_0 = c\tilde{u}_0, \tag{B1d}$$

$$y\tilde{u}_0 + \partial_y \tilde{p}_0 = 0, \quad \text{and} \tag{B1e}$$

$$\tilde{u}_0 + \partial_y \tilde{v}_0 = 0. \tag{B1f}$$

This is a system of ordinary differential equations with real valued coefficients that, since we have shown that all waves are stable, will have real eigenvalues c. The background meridional velocity V and the zonal wavenumber of the perturbation k only appear in the

combination V/k. This scaling feature means that a meridional circulation with magnitude $|V| = 2$ will have the same effect on a wavenumber $k = 4$ wave as would a circulation of $|V| = 1$ on a wavenumber $k = 2$ wave; this reduces the size of the parameter space.

REFERENCES

Biello, J., and A. Majda, 2004: The effect of meridional and vertical shear on the interaction of equatorial baroclinic and barotropic Rossby waves. *Stud. Appl. Math.*, **112**, 341–390, https://doi.org/10.1111/j.0022-2526.2004.01518.x.

——, and ——, 2010: Intraseasonal multi-scale moist dynamics of the tropical atmosphere. *Commun. Math. Sci.*, **8**, 519–540, https://doi.org/10.4310/CMS.2010.v8.n2.a11.

Charney, J., 1947: The dynamics of long waves in a baroclinic westerly current. *J. Meteor.*, **4**, 135–162, https://doi.org/10.1175/1520-0469(1947)004<0136:TDOLWI>2.0.CO;2.

Dias, J., and O. Pauluis, 2009: Convectively coupled waves propagating along an equatorial ITCZ. *J. Atmos. Sci.*, **66**, 2237–2255, https://doi.org/10.1175/2009JAS3020.1.

Eady, E., 1949: Long waves and cyclone waves. *Tellus*, **1**, 33–52, https://doi.org/10.3402/tellusa.v1i3.8507.

Gill, A., 1980: Some simple solutions for heat-induced tropical circulation. *Quart. J. Roy. Meteor. Soc.*, **106**, 447–462, https://doi.org/10.1002/qj.49710644905.

Guo, Y., X. Jiang, and D. E. Waliser, 2014: Modulation of the convectively coupled Kelvin waves over South America and the tropical Atlantic Ocean in association with the Madden–Julian oscillation. *J. Atmos. Sci.*, **71**, 1371–1388, https://doi.org/10.1175/JAS-D-13-0215.1.

Kalnay, E. A., 1996: The NCEP/NCAR Reanalysis 40-Year Project. *Bull. Amer. Meteor. Soc.*, **77**, 437–471, https://doi.org/10.1175/1520-0477(1996)077<0437:TNYRP>2.0.CO;2.

Kiladis, G. N., M. C. Wheeler, P. T. Haertel, K. H. Straub, and P. E. Roundy, 2011: Convectively coupled equatorial waves. *Rev. Geophys.*, **47**, RG3004, https://doi.org/10.1029/2008RG000266.

Liu, F., and B. Wang, 2013: Mechanisms of global teleconnections associated with the Asian summer monsoon: An intermediate model analysis. *J. Climate*, **26**, 1791–1806, https://doi.org/10.1175/JCLI-D-12-00243.1.

Majda, A., and J. Biello, 2003: The nonlinear interaction of barotropic and equatorial baroclinic Rossby waves. *J. Atmos. Sci.*, **60**, 1809–1821, https://doi.org/10.1175/1520-0469(2003)060<1809:TNIOBA>2.0.CO;2.

——, and R. Klein, 2003: Systematic multiscale models for the tropics. *J. Atmos. Sci.*, **60**, 393–408, https://doi.org/10.1175/1520-0469(2003)060<0393:SMMFTT>2.0.CO;2.

Mapes, B., 2000: Convective inhibition, subgrid-scale triggering energy, and stratiform instability in a toy tropical wave model. *J. Atmos. Sci.*, **57**, 1515–1535, https://doi.org/10.1175/1520-0469(2000)057<1515:CISSTE>2.0.CO;2.

Matsuno, T., 1966: Quasi-geostrophic motions in the equatorial area. *J. Meteor. Soc. Japan*, **44B**, 25–43, https://doi.org/10.2151/jmsj1965.44.1_25.

Ogrosky, H. R., and S. N. Stechmann, 2016: Identifying convectively coupled equatorial waves using theoretical wave eigenvectors. *Mon. Wea. Rev.*, **144**, 2235–2264, https://doi.org/10.1175/MWR-D-15-0292.1.

Powell, S. W., and R. A. Houze Jr., 2015: Effect of dry large-scale vertical motions on initial MJO convective onset. *J. Geophys. Res. Atmos.*, **120**, 4783–4805, https://doi.org/10.1002/2014JD022961.

Rayleigh, J., 1880: On the stability or instability of certain fluid motions. *Proc. London Math. Soc.*, **9**, 57–70.

Roundy, P. E., and G. N. Kiladis, 2006: Observed relationships between oceanic Kelvin waves and atmospheric forcing. *J. Climate*, **19**, 5253–5272, https://doi.org/10.1175/JCLI3893.1.

Sakai, S., 1989: Rossby–Kelvin instability—A new type of ageostrophic instability caused by a resonance between Rossby waves and gravity waves. *J. Fluid Mech.*, **202**, 149–176, https://doi.org/10.1017/S0022112089001138.

Schneider, T., 2006: The general circulation of the atmosphere. *Annu. Rev. Earth Planet. Sci.*, **34**, 655–688, https://doi.org/10.1146/annurev.earth.34.031405.125144.

Sobel, A. H., and D. Kim, 2012: The MJO–Kelvin wave transition. *Geophys. Res. Lett.*, **39**, L20808, https://doi.org/10.1029/2012GL053380 .

Takayabu, Y. N., 1994: Large-scale cloud disturbances associated with equatorial waves. Part 1: Spectral features of the cloud disturbances. *J. Meteor. Soc. Japan*, **72**, 433–449, https://doi.org/10.2151/jmsj1965.72.3_433.

Wang, B., and X. Xie, 1996: Low-frequency equatorial waves in vertically sheared zonal flow. Part I: Stable waves. *J. Atmos. Sci.*, **53**, 449–467, https://doi.org/10.1175/1520-0469(1996)053<0449:LFEWIV>2.0.CO;2.

Wheeler, M., and G. Kiladis, 1999: Convectively coupled equatorial waves: Analysis of clouds and temperature in the wavenumber–frequency domain. *J. Atmos. Sci.*, **56**, 374–399, https://doi.org/10.1175/1520-0469(1999)056<0374:CCEWAO>2.0.CO;2.

——, ——, and P. Webster, 2000: Large-scale dynamical fields associated with convectively coupled equatorial waves. *J. Atmos. Sci.*, **57**, 613–640, https://doi.org/10.1175/1520-0469(2000)057<0613:LSDFAW>2.0.CO;2.

Xie, X., and B. Wang, 1996: Low-frequency equatorial waves in vertically sheared zonal flow. Part II: Unstable waves. *J. Atmos. Sci.*, **53**, 3589–3605, https://doi.org/10.1175/1520-0469(1996)053<3589:LFEWIV>2.0.CO;2.

Zhang, C., 2005: Madden–Julian oscillation. *Rev. Geophys.*, **43**, RG2003, https://doi.org/10.1029/2004RG000158.